



# Designing linear lattices for round beam in electron storage rings using the solution by linear matrices analysis

Yongjun Li (李永军) <sup>1,\*</sup> and Robert Rainer <sup>1</sup>

<sup>1</sup>*Brookhaven National Laboratory, Upton 11973, New York, USA*

For some synchrotron light source beamline applications, a round beam is preferable to a flat one. A conventional method of obtaining round beam in an electron storage ring is to shift its tune close to a linear difference resonance. The linearly coupled beam dynamics is analyzed with perturbation theories, which have certain limitations. In this paper, we adopt the Solution by LInear Matrices (SLIM) analysis to calculate exact beam sizes to design round beam lattices. The SLIM analysis can deal with a generally linearly coupled accelerator lattice. The effects of various coupling sources on beam emittances and sizes can be studied within a self-consistent frame. Both the on- and off-resonance schemes to obtain round beams are explained with examples. The SLIM formalism for two widely used magnet models: combined-function bending magnets, and planar wigglers and undulators, is also derived.

## I. INTRODUCTION

Round beam rather than a flat one is preferable for some beamline applications in the synchrotron light source community. Concurrently, an increased vertical beam size can significantly improve beam lifetime as well, particularly in extremely low emittance rings. Therefore, some future diffraction-limited light sources, such as ALS-U [1] and APS-U [2], are planning to operate with a round beam mode. Most of light source rings only have horizontal bending magnets, which leads to an intrinsically flat beam. Either dedicated devices, such as skew quadrupoles, or some imperfections in magnets, such as normal quadrupole roll errors, can couple the beam motion transversely. Conventionally, a geometric round beam in an electron machine is obtained by: (1) equally distributing the natural horizontal emittance into the horizontal and vertical planes  $\epsilon_x = \epsilon_y$  through shifting the machine's tune close to a linear difference resonance  $\nu_x - \nu_y - n = 0$ , with  $n$  an integer, (2) adjusting the envelop Twiss functions so that  $\beta_x = \beta_y$  at the locations of radiators. Here we also assume that radiators are located at non-dispersive sections, because achromat lattices are often adopted for light source rings. The beam emittances and sizes for this on-resonance coupling case were often analyzed with perturbation theories, such as [3–5] etc. However, when the linear coupling is sufficiently strong, such perturbation analyses might not be accurate any longer and a more accurate analysis might be considered necessary.

In the presence of linear coupling, the uncoupled 2-dimensional Courant-Snyder parameterization [6] can be generalized to the 4-dimensional coupled motion. Such parameterizations, proposed by Ripken and his colleagues [7, 8] and further developed by Lebedev and Bogacz [9] are already available. There are also some other exact parameterizations [10–12]. These analyses

only deal with linear Hamiltonian systems, the radiation damping and quantum excitation diffusion for electron beams are not considered. Therefore, the equilibrium emittance for electron storage rings has not been derived here. Instead, the following emittance re-distribution approximation [4],

$$\epsilon_x = \frac{1 + 2k^2}{1 + 4k^2} \epsilon_{x,0}, \quad \epsilon_y = \frac{2k^2}{1 + 4k^2} \epsilon_{x,0} \quad (1)$$

is often used. Here  $k = \frac{|\kappa|}{\Delta\nu}$ ,  $\kappa$  is the well-known coupling coefficient given in ref. [4, 13],  $\Delta\nu = \nu_x - \nu_y - p$  is the distance from the resonance,  $\epsilon_{x,0}$  is the horizontal emittance for the uncoupled motion, and the natural vertical emittance  $\epsilon_{y,0}$  is negligible. Eq. (1) is only valid by assuming: (i) coupling coefficient  $\kappa$  are sufficiently weak to be considered as perturbations, (ii) the total transverse emittance remains as a constant, and (iii) the coupling is caused by a single isolated resonance. (iv) the vertical dispersion is negligible. Exact computations as shown later in this paper indicate that the approximation in Eq. (1) can break down when these assumptions are violated, particularly when vertical dispersion is blown up.

In this paper, to design round beam lattices for light source rings, we adopt an exact and self-consistent analysis – the Solution by LInear Matrices (SLIM) technique, developed by Chao back in the 1970–1980s [14–16]. This analysis can yield fruitful results such as the trajectory of the electron distribution center and the beam sizes and shapes in phase space. Linear coupling effects among the horizontal, vertical, and longitudinal motions are included in a straightforward manner even without introducing the auxiliary Twiss functions. An alternate, and also exact approach is to calculate the coupled synchrotron-radiation integrals [17], which was implemented in the code SAD [18] and AT [19], which could also be used for this purpose. We used AT and SLIM to compute a same coupled NSLS-II lattice and confirmed that their emittance computations are equivalent.

The remainder of this paper is outlined as follows: Sect. II briefly explains the principle of the SLIM anal-

\* email: yli@bnl.gov

ysis. Sect. III introduces the linear couplings due to two random errors: Subsect. III A reviews the methods to take closed orbit errors into account; and the effect of normal quadrupole roll errors is investigated in Subsect. III B. Sect. IV explains two round beam schemes, i.e., on- and off-resonance optics using examples. In Sect. V, we explain the strategies on the orbit and optics correction for different coupled lattice schemes, and indicate the direct tracking-based dynamic aperture optimization can still be used for nonlinear dynamics design. Some discussion and a brief summary is given in Sect. VI. The formalism of two commonly used magnetic devices, combined-function bending magnets and planar wigglers and undulators, are given in the Appendix A and B respectively.

## II. SLIM AND AUXILIARY TWISS FUNCTIONS

The detailed SLIM formalism can be found in the references [14–16, 20] and has been implemented in some accelerator codes, such as MAD-X [21]. Here we will briefly explain its basic principles. It deals with the motion of a charged particle in a linear electromagnetic device by purely using their transport matrices. First, symplectic one-turn linear matrices for a storage ring are used to compute the eigenvalues and eigenvectors. The eigenvalues indicate whether the linear motion is stable or not, and provides the fractional parts of the tunes when the motion is stable. The eigenvectors evolving along the ring provide information about closed orbit, beam size, etc. For electron rings, non-symplectic one-turn matrices including the radiation damping are used to compute the damping rates. Then equilibrium emittances are obtained by balancing the quantum diffusion and radiation damping in all radiating magnets around the ring. The particle distributions within a bunch along the ring can be given with 21 independent second moments. In the presence of linear couplings, no approximation is needed and therefore, the computations are exact. The ring's global emittances and the local  $s$ -dependent beam sizes are derived within a self-consistent frame.

When there is no linear coupling, two SLIM's second moments  $\langle xx \rangle, \langle yy \rangle$  were confirmed to agree with the beam sizes obtained with Sands's formalism [22] using the Courant-Snyder parameterization. Throughout this paper the National Synchrotron Light Source II (NSLS-II) double bend achromat (DBA) bare lattice was used for the proof of concept. Fig. 1 shows the magnet layout of its one supercell composed of two mirror symmetrical DBA cells, and the uncoupled beam sizes along  $s$ , computed using these two methods.

Linear coupling can then be introduced into the lattice by inserting two 0.2  $m$  long skew quadrupoles inside each supercell as shown in Fig. 2. The first family of skew quadrupoles ( $SQ_1$ ) are located within the achromat dispersive sections, while the second family ( $SQ_2$ ) are located at the original dispersion-free sections. As a

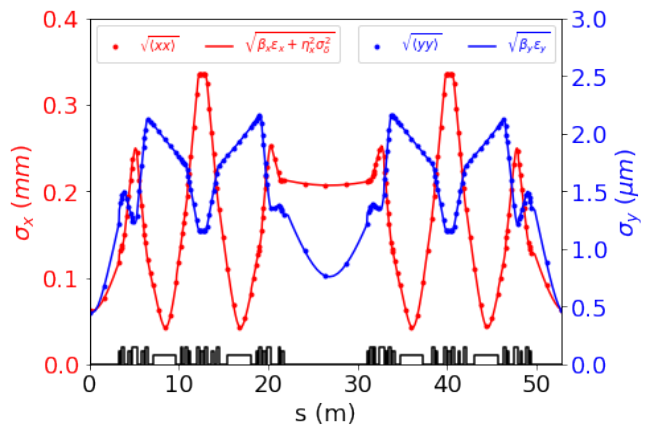


Figure 1. NSLS-II DBA lattice magnet layout in a supercell. The beam sizes are represented with the 2nd moments in the SLIM analysis (dots) and the Courant-Snyder parameters (lines) for the uncoupled motion agrees with each other. Note that the vertical axes' scales and units for the horizontal (left) and vertical (right) beam sizes are different.

numerical experiment, all 30 skew quads were set with the same normalized focusing value  $|K_1| = \left| \frac{1}{B\rho} \frac{\partial B_y}{\partial y} \right|$  but given alternating polarities (+, -, + ...) along the ring. Here  $B\rho$  is the beam rigidity. The variation of the emittances with  $|K_1|$  can then be computed with the SLIM analysis as shown in Fig. 3. The vertical emittance is observed to grow fast with the coupling strength, which leads to the sum of two emittances becoming variable and no longer constant. Eq. (1) is only valid when the coupling coefficient  $\kappa$  is sufficiently small.

No auxiliary Twiss functions are needed in the SLIM analysis as the particle distributions are obtained by computing 21 independent second moments projected on the corresponding subspaces. However, it is worth noting are these coupled Twiss functions parameterized with Ripken method [7, 8] are still useful in interpreting the same physics meanings. Given an equilibrium emittances  $\epsilon_{x,y}$  and energy spread  $\sigma_\delta$ , the beam size along the ring can also be computed with the following formula [23] as illustrated in Fig. 2.

$$\sigma_{x,y}^2 = \beta_{I,(x,y)} \epsilon_I + \beta_{II,(x,y)} \epsilon_{II} + \eta_{x,y}^2 \sigma_\delta^2. \quad (2)$$

Using Eq. (2), we can further understand the blow-up of vertical beam size by decomposing it into three components as shown in Fig. 4. When the dispersion is coupled from the horizontal plane to the vertical plane, it generates a considerable amount of mode II emittance  $\epsilon_{II}$  and introduces local vertical energy oscillation  $\eta_y \sigma_\delta$  as well. In the meantime, the coupled  $\beta_{I,y}$  function can also generate a contribution  $\beta_{I,y} \epsilon_I$ . When the vertical dispersion is sufficiently large, even no significant beam size change is observed in the horizontal plane, a new equilibrium state is formed in the vertical plane.

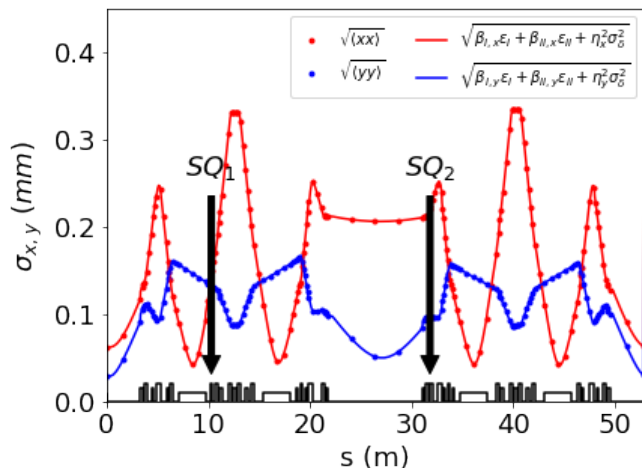


Figure 2. Beam sizes obtained with the SLIM analysis (dots) and Ripken parameterization (line) in the presence of linear coupling. The locations of two skew quadrupoles are marked. By assigning them the same  $|K_1|$  value, but alternating polarities along the ring, the vertical emittance and overall beam sizes will blow up. The dotted lines are the second moments obtained with the SLIM analysis, and the solid lines are computed with the coupled Twiss functions in Ripken parameterization. Nevertheless, for both cases, the equilibrium emittances  $\epsilon_{I,II}$  and energy spread  $\sigma_\delta$  need to be computed with the SLIM analysis first.

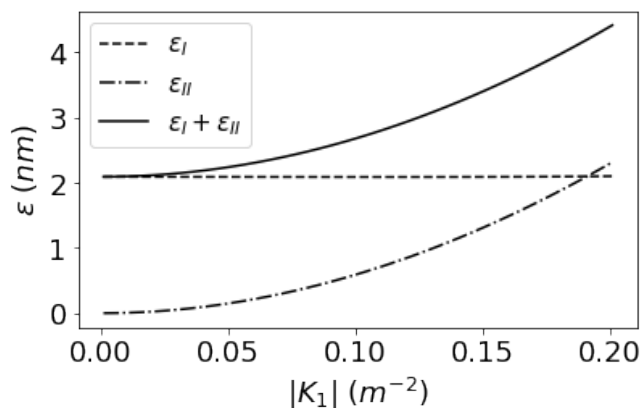


Figure 3. The correlation between the transverse emittances and the skew quadrupoles' strength  $|K_1|$ . The vertical emittance (the dot-dash line) grows faster than the reduction of the horizontal emittance (the dashed line). The total emittance is not constant when the coupling becomes strong, which leads to the breakdown of Eq. (1).

### III. COUPLING FROM RANDOM ERRORS

Linear coupling can be from not only dedicated magnets, such as skew quadrupoles and solenoids, but some random errors. In this section, the effects of two primary sources, the vertical closed orbit through sextupoles and the roll errors of normal quadrupoles, are discussed.

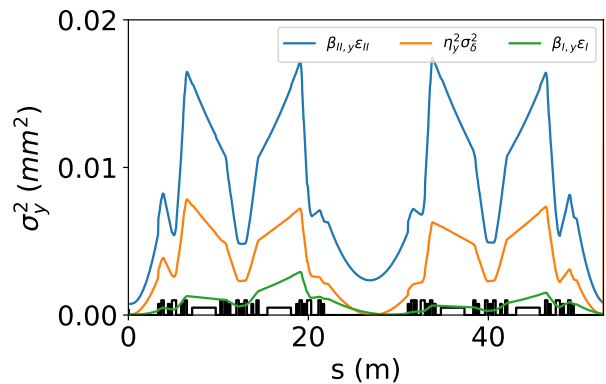


Figure 4. Vertical beam size decomposition: coupled vertical dispersion (1) generates a considerable amount of mode II emittance contribution, which contributes  $\beta_{II,y}\epsilon_{II}$  (blue), (2) introduces local energy oscillation, which contributes  $\eta_y^2\sigma_\delta^2$  (yellow); (3) the coupled  $\beta_{I,y}$  function couples some mode I emittance, which contributes  $\beta_{I,y}\epsilon_I$  (green).

#### A. Closed orbit errors

In reality, small misalignments and magnet imperfections are unavoidable. Therefore, when circulating beam reaches an equilibrium distribution around a closed orbit, it always differs, at least slightly, from the design orbit. In this section, the technique for studying the effect of closed orbit on beam size is briefly explained. Closed orbit, if it exists, can be accurately obtained by performing an iterative one-turn 6-dimensional tracking till a convergence is reached. This method is widely used in many existing lattice codes, such as ELEGANT [24] and MAD [25]. Alternatively, the SLIM analysis adds a seventh component, which is always a unitary constant 1, to expand one-turn transport matrices to a  $7 \times 7$  format. The upper-left  $6 \times 6$  corners of these matrices are the usual transport matrices. The 7<sup>th</sup> row of all M matrices is always filled with  $[0 \ 0 \ 0 \ 0 \ 0 \ 0 \ 1]$ . The remaining upper-right  $6 \times 1$  is the cause of orbit distortion, such as dipole errors. In this case, the closed orbit corresponds to the eigenvectors with eigenvalues of 1. The nonlinear kicks from nonlinear multipoles can also be accounted for by iteratively updating the transport matrices around the local closed orbit to reach a convergence.

Once the closed orbit is obtained, the transport matrix of each magnet needs to be updated with the reference to it. Thick-lens off-axis transport matrices can be computed in different ways. A simple kick-drift model is often used to obtain an approximation of thick elements. First, a thick element is sliced into multiple pieces, e.g.,  $n$  pieces. Each piece is approximated by two components of drift with a thin-lens kick in-between. By concatenating those slices sequentially, a thick model is obtained. For example, a thick lens sextupole can be approximated as the sequential products of the following kick-drift ma-

trices,

$$R_{co,i} = M_d M_k M_d, \quad (3)$$

with

$$M_d = \begin{bmatrix} 1 & \frac{l_s}{2} & 0 & 0 & 0 & 0 \\ 0 & 1 & 0 & 0 & 0 & 0 \\ 0 & 0 & 1 & \frac{l_s}{2} & 0 & 0 \\ 0 & 0 & 0 & 1 & 0 & 0 \\ 0 & 0 & 0 & 0 & 1 & \frac{l_s}{2\gamma^2} \\ 0 & 0 & 0 & 0 & 0 & 1 \end{bmatrix},$$

and

$$M_k = \begin{bmatrix} 1 & 0 & 0 & 0 & 0 & 0 \\ -\lambda x_{0,i} & 1 & \lambda y_{0,i} & 0 & 0 & \frac{\lambda}{2}(x_{0,i}^2 - y_{0,i}^2) \\ 0 & 0 & 1 & 0 & 0 & 0 \\ \lambda y_{0,i} & 0 & \lambda x_{0,i} & 1 & 0 & -\lambda x_{0,i} y_{0,i} \\ -\frac{\lambda}{2}(x_{0,i}^2 - y_{0,i}^2) & 0 & \lambda x_{0,i} y_{0,i} & 0 & 1 & 0 \\ 0 & 0 & 0 & 0 & 0 & 1 \end{bmatrix}.$$

Here  $R_{co,i}$  stands for the  $i^{\text{th}}$  slice's matrix around the local closed orbit coordinates  $(x_{0,i}, y_{0,i})$ ,  $\lambda = \frac{l_s}{B\rho} \frac{\partial^2 B_y}{\partial^2 x}$  is the normalized focusing integral of this slice, and  $\gamma$  is the relativistic factor. When each slice's  $l_s$  is reasonably small, the thick-lens  $R_{co} = R_{co,n} \cdots R_{co,2} R_{co,1}$  will be sufficiently accurate. Since the kick-drift scheme is adopted, such thick-lens matrices are automatically symplectic. This  $2^{\text{nd}}$ -order thick-lens model has been adopted in our investigation. More complicated high order kick-drift schemes, as explained in ref. [26], are also available.

Another method to obtain a thick element's off-axis transport matrix is to compute its higher order on-axis matrices first, then the following truncated Taylor map [27] is used,

$$R_{co} = R + 2TX_0 + 3UX_0^2 + \cdots, \quad (4)$$

where  $X_0$  represents the 6-dimensional closed orbit vector at the magnet entrance and  $R, T, U$  are the  $1^{\text{st}} - 3^{\text{rd}}$  order on-axis transport matrices which can be obtained with the truncated power series algorithm [28]. However, the truncated map is usually not perfectly symplectic, and can introduce an artificial damping or excitation. A symplectification process might be considered, if needed.

From Eq. (3), a vertical offset through sextupoles introduces linear coupling (non-zero  $m_{23}$  and  $m_{41}$ ). In modern high brightness light source rings, strong sextupoles are needed to correct chromaticity and enlarge dynamic aperture. Small closed orbit errors might introduce some coupling which can blow up the vertical emittance as shown in Fig. 5. The summation of transverse emittances increases gradually with the amplitude of vertical orbit. The idea of the constant emittance assumption from Eq. (1) appears valid only when the root-mean-square (RMS) closed orbit error is less than about  $200\mu\text{m}$  for the NSLS-II storage ring.

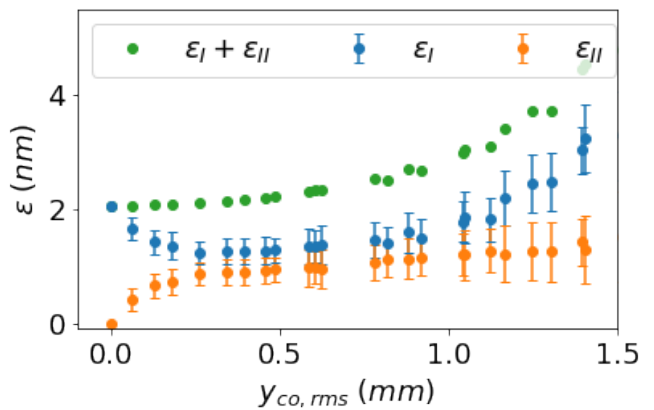


Figure 5. Correlation between the emittances and RMS vertical orbit distortions  $y_{co,rms}$ . With gradually increasing orbit distortion, a very flat beam becomes a near-round one. When the closed orbit distortion is sufficiently large, it becomes flat (and tilted) but with larger emittances. The total emittance is observed to be blown up, albeit rather slowly.

The above computation is carried out when the machine's fractional tune (0.22/0.26) is not near the difference resonance. When the uncoupled tune is close to the difference resonance  $\nu_x - \nu_y = n$ , the vertical beam emittance can be easily increased as will be discussed in Sect. IV A.

## B. Normal quadrupole roll errors

Another linear coupling source is from the random normal quadrupole roll errors. Quadrupoles can be aligned within several hundreds of microradians roll angles using the modern alignment techniques. If the linear tune is sufficiently separated from resonances, even though the total beam emittances are only slightly increased (about 1-2%), a significant part of the transverse emittance can be gradually redistributed to the vertical plane, as shown in Fig. 6. While the machine's tune is sufficiently close to a difference resonance, even small roll errors can easily couple the transverse motion. This is the most common way to obtain an approximately round beam, Although it can be explained well with perturbation theory, this particular case will be re-analyzed exactly with the SLIM technique in Sect. IV A.

## IV. TWO ROUND BEAM SCHEMES

Thus far, we have explained how to compute exact beam emittances and sizes in the presence of various coupling sources using the SLIM analysis. To obtain round beam in an electron storage ring, its vertical emittance needs to be blown up with either dedicated coupling elements (skew quadrupoles, solenoids), or by shifting the



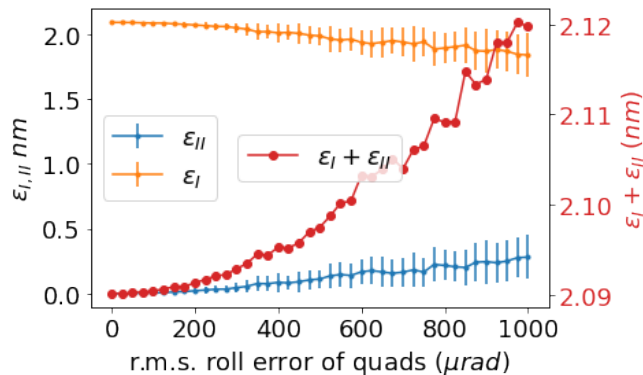


Figure 6. Emittance variation with quadrupole roll errors when the machine's tune (0.22/0.26) is off a difference resonance.

machine's tunes close to a difference resonance, and letting random coupling errors (such as quadrupole roll errors) to couple the emittances transversely. Below we quantitatively investigate two schemes with examples.

### A. Round beam with on-resonance tune

Currently, the most common method to obtain round beam is by shifting the machine's tune close to a difference resonance. With this on-resonance scheme, random imperfections are usually sufficient to couple the transverse motion. Because orbit displacements through sextupoles centers can be well controlled using the beam-based-alignment technique [29, 30], quadrupoles' roll errors are regarded as the primary coupling sources, which are often at a level of several hundred microradians.

Although this on-resonance scheme can be explained with the perturbation theory, we re-investigated it with the exact SLIM analysis. Our design goal is to make the beam to be round at the short straight centers (SSC). First, the local quadrupoles  $QL_{1-3}$  there were re-tuned to let the local eigenvectors absolute values to be close (or the coupled  $\beta_{(x,y),(I,II)}$  functions to be close if one prefers to use Eq. (2) instead.) Then the quadrupoles in the long straight sections  $QH_{1-3}$  were tuned to shift the fractional tune close to a difference resonance. Here we assumed the RMS roll angles for quadrupoles is  $500 \mu rad$ , which can be easily achieved with the current alignment technique. The needed adjustments on quadrupoles settings as listed in Tab. I can switch the nominal lattice to an on-resonance round beam lattice. The corresponding beam emittances, fractional tune and beam sizes (at SSCs) are also listed there.

The eigen-emittances and beam sizes' variation with the quadrupole roll angles are illustrated in Fig. 7 and Fig. 8 respectively. Because quadrupole roll errors are random, the corresponding beam emittances and sizes have some statistical fluctuations as represented by error bars there. These figures illustrate the needed

Table I. Parameters from flat beam to round beam with on-resonance tune

name	original value	new value	unit
$K_{1,QL_1}$	-1.61785	-1.39864	$m^{-2}$
$K_{1,QL_2}$	1.76477	1.73601	$m^{-2}$
$K_{1,QL_3}$	-1.51868	-1.58219	$m^{-2}$
$K_{1,QH_1}$	-0.64196	-0.62274	$m^{-2}$
$K_{1,QH_2}$	1.43673	1.42475	$m^{-2}$
$K_{1,QH_3}$	-1.75355	-1.76958	$m^{-2}$
R.M.S. quad. roll 0		500	$\mu rad$
$\epsilon_I/\epsilon_{II}$	2.096/0.0002	1.185/0.925	nm
$\nu_I/\nu_{II}$ <sup>a</sup>	0.22/0.26	<b>0.23/0.23</b>	1
$\sigma_x/\sigma_y$ <sup>b</sup>	62.08/0.45	<b>43.1/44.2</b>	$\mu m$

<sup>a</sup> fractional part

<sup>b</sup> averaged beam sizes observed at short straight centers

quadrupoles roll errors to get a geometric round beam. With the quadrupole settings in Tab. I, a RMS error greater than  $400 \mu rad$  will be sufficient to result in  $\sigma_x \approx \sigma_y$ . It is interesting to note that, the round beam size ( $\sim 44 \mu m$ ) is significantly greater than half of the uncoupled horizontal flat beam size ( $\sim 60 \mu m$ ) as seen in Fig. 8. It can be explained with Eq. (2): although two mode's emittances  $\epsilon_{I,II}$  are approximately equal, the sum of coupled  $\beta_{I,(x,y)} + \beta_{II,(x,y)}$  is greater than the uncoupled  $\beta_{(x,y)}$  as illustrated in Fig. 9. The beam sizes for one supercell with one specific random seed is illustrated in Fig. 10, which can be used for the beam lifetime estimation.

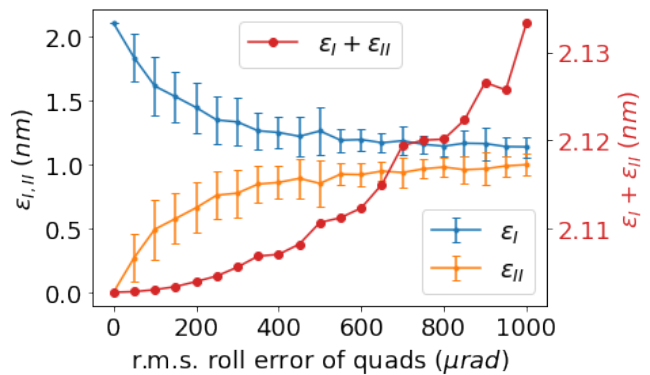


Figure 7. On-resonance scheme: correlation between the beam eigen-emittances with r.m.s. quadrupole roll errors when the ideal machine's tune is on a difference resonance. Each error bar is the standard deviation for 50 random seeds.

If quadrupoles are aligned accurately with smaller roll angles, eigen-emittances might not be equally distributed by the resonance coupling, i.e.,  $\epsilon_I > \epsilon_{II}$ . In this case, we can still tune the local quadrupoles ( $QL_{1-3}$ ) to make  $\beta_{(I,II),x} < \beta_{(I,II),y}$  correspondingly to get a geometric round beam.

Now we consider a more realistic situation by includ-

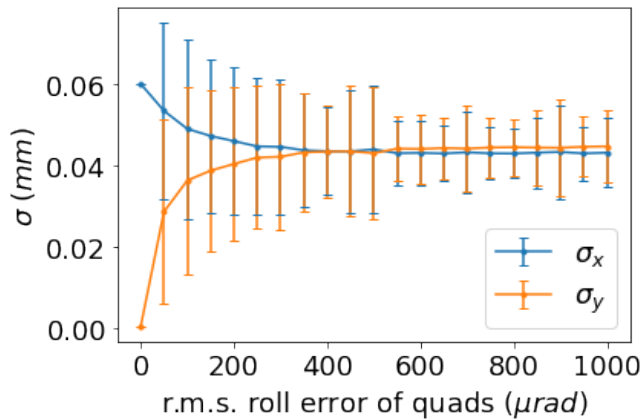


Figure 8. On-resonance scheme: correlation between the quadrupole roll errors and beam sizes at short straight centers when the ideal machine's tune is on a difference resonance. The error bar is the standard deviation of 50 random seeds.

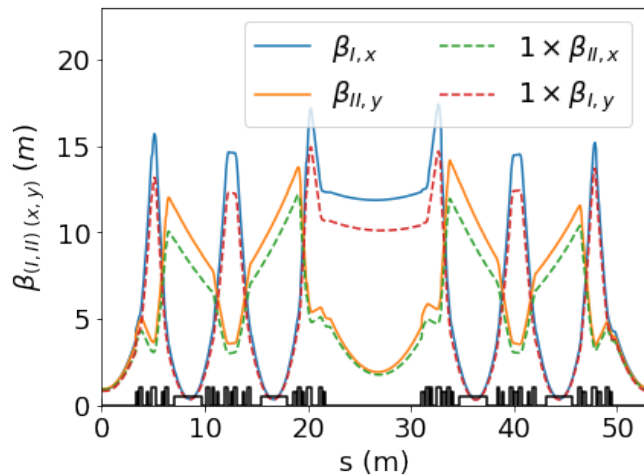


Figure 9. On-resonance scheme: four coupled  $\beta$  functions of one supercell for one random seed with  $500\mu\text{rad}$  quadrupole roll errors. The local  $\beta_{(I,II),x}$  at short straight sections are tuned close to  $\beta_{(I,II),y}$ , to obtain a geometric round beam there.

ing the closed orbit distortion. Thus the skew quadrupole components due to the vertical offsets through sextupoles can be taken into account. A simulation shows that the round beam profiles can still be maintained when the closed orbit errors are within a quite wide range (see Fig. 11). Once an even larger closed orbit distortion can drive the tune further away from the resonance, however, the beam profiles will gradually become flatter. Usually the closed orbit can be well controlled after the beam-based alignment technique is implemented, this error shouldn't be a concern.

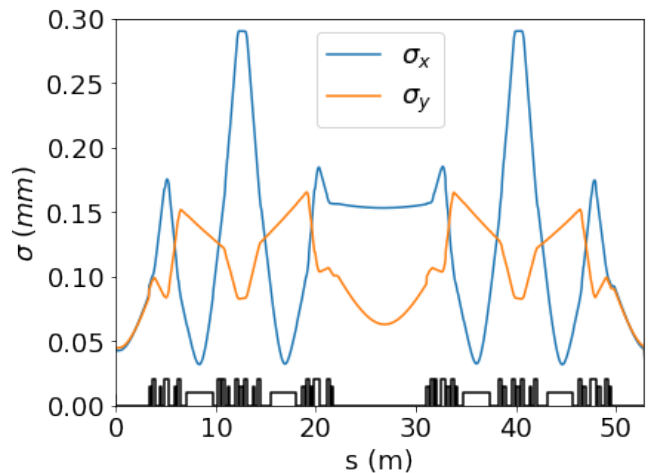


Figure 10. On-resonance scheme: horizontal and vertical beam sizes of one supercell for one specific random seed with  $500\mu\text{rad}$  quadrupole roll errors. Such data can be used for the beam lifetime estimation.

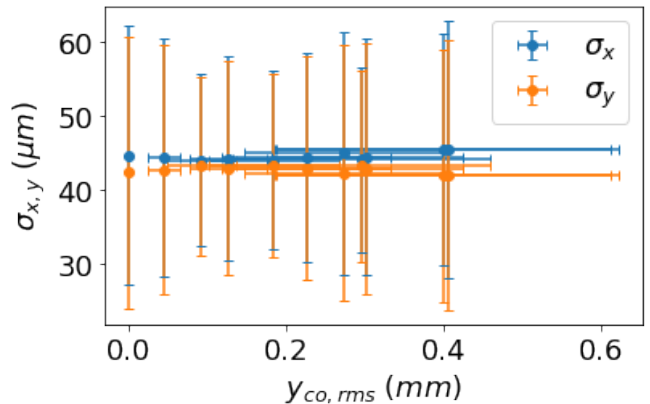


Figure 11. On-resonance scheme: round beam profile can be maintained with gradually increased closed orbit errors when the machine's tune stays near a difference resonance.

## B. Round beam with off-resonance tune

The second scheme to obtain round beam would be to use some strong skew/tilted quadrupoles (or solenoids), which would allow the machine's tune to stay off resonances. In this case, the perturbation theory is not applicable. To obtain round beam at specific locations, the linear lattice design can be summarized as an optimization problem:

1. Assign some magnet's focusing strengths (such as normal and skew quadrupoles)  $K_1$ , and/or tilt angles  $\phi$  as knobs.
2. Simultaneously minimize:
  - (a)  $\epsilon_I$ ;
  - (b)  $\epsilon_{II}$ ;

(c)  $|\frac{\sigma_y}{\sigma_x} - 1|$  at specific  $s$  locations.

3. subject to the following constraints:

- (a) the existence of stable linear solutions;
- (b) the fractional tune is sufficiently away from low order resonances;
- (c)  $\epsilon_{I,II} < \epsilon_{threshold}$
- (d) the tilt angle  $|\theta_{xy}| < \theta_{threshold}$ ;
- (e)  $K_1 \in [K_{1,min}, K_{1,max}]$ ;
- (f)  $|\frac{\sigma_y}{\sigma_x} - 1| < d$  at specific  $s$  locations;

Here, the stable linear solution constraint means that three eigenvalues of the one-turn symplectic matrix must stay on the complex unity circle,  $\epsilon_{threshold}$  is the emittance threshold to guarantee the required brightness,  $\tan 2\theta_{xy} = \frac{2\langle xy \rangle}{\langle xx \rangle - \langle yy \rangle}$  defines the tilt angle for the  $x - y$  beam profile relative to the horizontal axis,  $d$  represents an allowed tolerance for the beam to be a perfectly round shape. This linear lattice design eventually needs to be optimized iteratively after taking the dynamic aperture and energy acceptance into account, but was not covered in this paper.

A possible linear solution for the NSLS-II ring is listed in Tab. II. Three families of quadrupoles  $QL_{1-3}$ , and two families of skew quadrupoles  $[SQ_1, SQ_2]$  are used. The beam size for one supercell is illustrated in Fig. 12.

Table II. Parameters from flat beam to round beam for off-resonance tune

Name	original value	new value	unit
$K_{1,QL1}$	-1.61785	-1.23000	$m^{-2}$
$K_{1,QL2}$	1.76477	1.70791	$m^{-2}$
$K_{1,QL3}$	-1.51868	-1.61387	$m^{-2}$
$K_{1,SQ1}$	0	0.085	$m^{-2}$
$K_{1,SQ2}$	0	-0.090	$m^{-2}$
$\epsilon_I/\epsilon_{II}$	2.096/0.0002	2.095/1.460	$nm$
$\nu_I/\nu_{II}$ <sup>a</sup>	0.22/0.26	<b>0.59/0.66</b>	1
$\sigma_x/\sigma_y$ <sup>b</sup>	62.08/0.45	<b>55.5/53.8</b>	$\mu m$

<sup>a</sup> fractional part

<sup>b</sup> observed at short straight centers

Once the imperfections of magnets and the misalignments are accounted for, beam will reach an equilibrium around a closed orbit with random quadrupole roll errors. A large quadrupole roll errors and closed orbit distortions could overstretch and tilt the round beams. For example, a simulation studying the deformation of a round beam due to vertical closed orbit distortions is shown in Fig. 13. For this particular lattice, since its tune is away from the difference resonance, the profile of the round beam is not noticeably sensitive to closed orbit distortions if they can be constrained to within  $100 - 200\mu m$ .

Recently a hybrid flat-round beam scheme [31] is being under investigation for a steady-state microbunching [32]

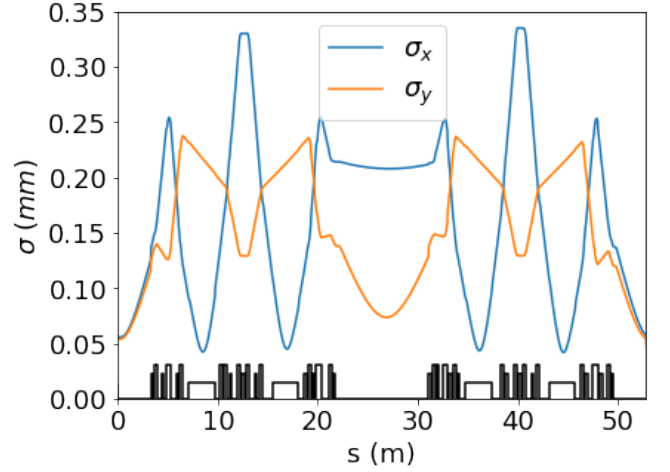


Figure 12. Off-resonance scheme: horizontal and vertical beam sizes of one supercell.

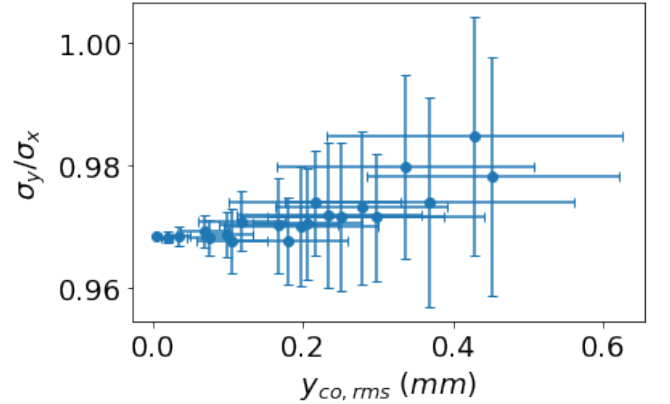


Figure 13. Off-resonance scheme: ratio of the vertical and horizontal beam sizes varies with the vertical closed orbit distortions. The initial ratio of transverse beam sizes is  $\sigma_y/\sigma_x \approx 0.97$ , then a closed orbit that is increased gradually can slightly stretch the beam  $x - y$  profile vertically. Each error bar represents the standard deviation of 20 random seeds.

ring. A similar idea has been studied using a different method [33] for a diffraction-limited light source ring. The schematic diagram of this hybrid flat-round beam mode for a storage ring is illustrated in Fig. 14, in which a pair of coupling elements are used to generate a local closed section with a round beam, while maintaining a flat beam in the rest part of the ring. Obviously this scheme is also an off-resonance scheme. Even a fully coupling beam is limited within a section, once there exist radiation elements, such as dipoles, inside, it changes the mode I emittance in the “flat beam” part of the ring, which can be exactly analyzed with the SLIM technique.

It is worth to note that the off-resonance scheme is more robust to random errors than the on-resonance one by comparing Fig. 11 and 13. The reason is simply be-

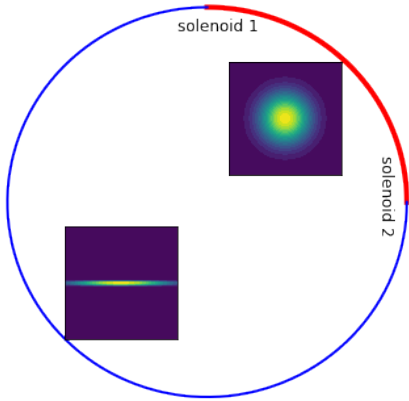


Figure 14. Schematic diagram of a hybrid flat-round beam mode in a storage ring. A pair of solenoids are used to form a local closed section with a round beam (red arc), while maintaining a flat beam in the rest part of the ring (blue arc.)

cause the on-resonance scheme solely relies on the random errors amplified by the linear resonance. While the off-resonance scheme takes advantage of strong and dedicated linear coupling magnets and the tune is far away from the resonance.

## V. ORBIT AND OPTICS CORRECTION, AND DYNAMIC APERTURE

In this section, we briefly discuss two topics related to linear lattice design, i.e., orbit and linear optics characterization and correction, and dynamic aperture optimization.

### A. Orbit and linear optics control

Linear orbit and optics characterization and correction need to be implemented during beam commissioning and routine operation. For the on-resonance scheme, coupling sources are random, so that there is some uncertainty in real lattices, and no precise lattice models are available. The orbit response matrix for the various orbit control should be measured experimentally. The uncoupled linear optics could be characterized and corrected when the machine tune is sufficiently away the difference resonance, then some dedicated quadrupoles can be used to shift the tune close to the resonance.

For the off-resonance scheme, coupling sources are well-defined magnetic elements integrated into the lattice model. Traditional methods, such as linear optics from closed orbit (LOCO) [34], can be used to characterize the optics and identify needed corrections. The only difference is that the off-diagonal elements in orbit response matrix are not zeros any longer. Similarly coupled orbit

response matrix should be used for various orbit controls as well.

### B. Dynamic aperture

Sufficient dynamic aperture (DA) and local momentum aperture (LMA) are always required for carrying out high efficiency injection and achieving desired beam lifetime. For the on-resonance scheme, DA and LMA should be optimized when the tune is sufficiently away the difference resonance. After some global quadrupole knobs are used to move the tunes to the linear difference resonance, tracking can be used to check the DA degradation. The linear chromaticities should be adjusted to an desired value for both modes with sextupoles. After DA tracking, statistical analysis of the DA are needed to provide the reduction percentile contours [2]. If a significant degradation of DA and/or LMA is found, some further optimization on uncoupled lattice is needed.

For the off-resonance scheme, given a linear optics, direct tracking-based DA optimization techniques, such as [35–37], can be used to optimize nonlinear magnets configuration. First, the chromaticities should be adjusted to an desired value for both modes with sextupoles. Due to the existence of vertical dispersion, most sextupoles can contribute to the linear chromaticities. In our off-resonance scheme example, we used the least square method to correct the linear chromaticities. Then the response matrix of chromaticity with respect to sextupoles was decomposed to get its null vectors [38]. Various linear combination of those null vectors were added on sextupoles to optimize DA and LMA without changing linear chromaticities. Sufficient DAs were obtained as illustrated in Fig. 15. If the optimal solution can't satisfy the DA requirement, iteratively optimization for the linear optics should be considered necessary.

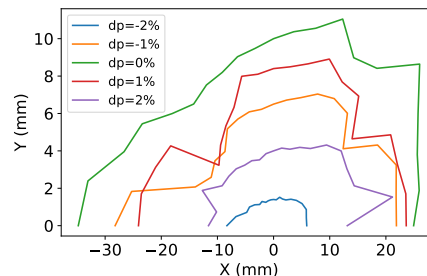


Figure 15. Optimized on- and off-momentum dynamic apertures for the off-resonance scheme as listed in Tab. II.

## VI. SUMMARY

Two schemes to obtain round beam, i.e., with machine's tune sitting on- or off- difference resonance, are



studied with the SLIM analysis. This exact analysis accounts for the linear coupling by calculating the quantum diffusion and radiation damping rate around a 6-dimensional closed orbit. The on-resonance scheme takes the advantage of the random imperfections to drive the beam to be coupled when the tune stays close to a difference resonance. This scheme is easy to implement in a real machine, however, beam profiles, coupled optics functions, and dispersions etc. have quite large and uncontrollable fluctuations. The off-resonance scheme can provide a more controllable and robust round beam, but needs to integrate dedicated magnets into the lattice to generate strong coupling.

In modern light source storage rings, high-harmonic cavities are often used to stretch the bunch longitudinally. Under desired conditions, the local potential well basin is flattened. Strictly speaking, if a linear focusing is missing from any dimension, the SLIM analysis cannot be applied. In this case, the head and tail of the bunch are still focused by the nonlinear potential well, but the bunch center will coast because there is no linear focusing at  $z = 0$ . To deal with this special case, an artificial, small linear RF focusing can be introduced. Although the bunches will have long longitudinal sizes, the transverse dynamics and energy spread computations are still correct because the longitudinal focusing is weak at most rings. However, this calculation will miss one class of effects, i.e., the nonlinear synchro-betatron coupling effects. When the longitudinal focusing comes purely from a nonlinear potential well, these nonlinear synchro-betatron effects could be significant. For cases like this, the SLIM analysis can still be used to design the linear lattice first, then detailed simulations are needed to study the nonlinear effects [31].

In real machine operations, maintaining round beam lattices can still be complicated and challenging. For example, when some users open or close their insertion device gaps, not only do the devices focusing properties change, but the equilibrium between the damping and quantum excitation changes simultaneously. Such changes are observed for all beamlines. Therefore, a feed-forward or feed-back system (or both) would be needed to stabilize machine's tune, coupling, local beam sizes etc. to account for these changes. As previously mentioned, the nonlinear beam dynamics is only mentioned lightly in this paper. Usually an iterative optimization between the linear and nonlinear lattice design would be needed once the SLIM analysis was deployed.

## ACKNOWLEDGMENTS

We would like to thank Prof. Alexander W. Chao (Stanford Uni.) and Dr. Xiujie Deng (Tsinghua Uni.) for invaluable discussions, reading the origin manuscript and code-sharing, Dr. P. Kuske for pointing out a misinterpretation on the perturbation theory. The supports and discussion from the NSLS-II colleagues are greatly

appreciated. This research used resources of the National Synchrotron Light Source II, a U.S. Department of Energy (DOE) Office of Science User Facility operated for the DOE Office of Science by Brookhaven National Laboratory under Contract No. DE-SC0012704.

## Appendix A: Combined-function bending magnets

Two magnet models commonly used in light source rings, combined-function bending magnets and wigglers and undulators, are not included in Chao's original literature. The appendices summarize their transport matrices, the corresponding changes when the radiation damping and closed orbit are considered. The quantum diffusion rate for planar wigglers and undulators are derived.

The Hamiltonian of combined function bending magnet is given in ref. [39]. Here a thick dipole is sliced into multiple pieces. The transport matrix around a closed orbit  $x_0, y_0$  for one slice can be approximated as,

$$R_{co,i} = M_d M_k M_d, \quad (A1)$$

with

$$M_k = \begin{bmatrix} 1 & 0 & 0 & 0 & 0 & 0 \\ -K_h l_s & 1 & 0 & 0 & 0 & K_h l_s x_0 + l_s h \\ 0 & 0 & 1 & 0 & 0 & 0 \\ 0 & 0 & K_1 l_s & 1 & 0 & -K_1 l_s x_0 \\ -K_h l_s x_0 - l_s h & 0 & K_1 l_s x_0 & 0 & 1 & 0 \\ 0 & 0 & 0 & 0 & 0 & 1 \end{bmatrix},$$

here  $M_d$  is the drift's transport matrix as already given in Eq. (3),  $K_h = K_1 + h^2$  with  $h = \frac{B_{y,0}}{B\rho}$  the reciprocal of bending radius. Correspondingly, after including the transverse gradient contribution, the radiation damping changes the diagonal  $m_{66}$  element as,

$$m_{66} = 1 - \frac{C_\gamma E^3 l_s (B_x^2 + B_y^2)}{\pi (B\rho)^2} \quad (A2)$$

here  $C_\gamma = 8.846 \times 10^{-5} m/GeV^3$  for electrons,  $B_y = B_{y,0} + \frac{\partial B_y}{\partial x} x_0$  and  $B_x = \frac{\partial B_x}{\partial y} y_0$  are the vertical and horizontal field seen by electrons at a closed orbit  $x_0, y_0$ . When calculating closed orbit, nonvanishing elements in the 7<sup>th</sup> column are

$$\begin{aligned} m_{67} &= -\frac{C_\gamma E^3 l_s (B_x^2 + B_y^2)}{\pi (B\rho)^2} \\ m_{27} &= \frac{m_{67} B_y l_s}{2 B\rho} \\ m_{47} &= \frac{m_{67} B_x l_s}{2 B\rho} \\ m_{77} &= 1. \end{aligned} \quad (A3)$$

## Appendix B: Planar insertion devices

Insertion devices such as wigglers and undulators are used as the main X-ray radiators on modern light source rings. In this appendix a planar Halbach type wiggler or undulator model [40] is integrated into the SLIM framework. The  $s$ -dependent vertical magnetic field of such a devices reads as,

$$B_y = \hat{B}_y \cosh(k_x x) \cosh(k_y y) \sin(ks), \quad (\text{B1})$$

Here  $k_x^2 + k_y^2 = k^2 = (\frac{2\pi}{\lambda_l})^2$ ,  $\lambda_l$  is the period length of the device,  $\hat{B}_y$  is the peak field in the vertical plane. The linear focusing of such type devices can be extracted as explained in ref. [41]. If the magnetic poles are sufficiently wide, the weak focusing in the horizontal plane is negligible, i.e.,  $k_x \approx 0$ , the nonvanishing linear transport matrix elements for one complete period are listed below.

$$\begin{aligned} m_{11} &= m_{22} = m_{55} = m_{66} = 1 \\ m_{12} &= \lambda_l \\ m_{33} &= m_{44} = \cos(\sqrt{K_y} \lambda_l) \\ m_{34} &= \frac{\sin(\sqrt{K_y} \lambda_l)}{\sqrt{K_y}} \\ m_{43} &= -\sqrt{K_y} \sin \sqrt{K_y} \lambda_l \\ m_{56} &= \lambda_l / \gamma^2. \end{aligned} \quad (\text{B2})$$

Here  $K_y = \frac{\hat{B}_y^2}{2(B\rho)^2}$ . Note that a complete wiggler and undulator period is an achromat system, therefore,  $m_{16} = m_{26} = 0$ . Other unlisted elements are all zeros. The radiation damping changes the diagonal element  $m_{66}$  for

one period as

$$m_{66} = 1 - \frac{C_\gamma E^3 \hat{B}_y^2 \lambda}{2\pi(B\rho)^2}. \quad (\text{B3})$$

The quantum diffusion rate for one period is

$$\langle |A_{\pm k}|^2 \rangle = C_L \frac{\gamma^5 |E_{k5}(s)|^2}{c\alpha_k} \frac{4\hat{B}_y^3 \lambda_l}{3\pi(B\rho)^3}, \quad (\text{B4})$$

here  $C_L = \frac{55}{48\sqrt{3}} \frac{r_e \hbar}{m_e}$ ,  $\hbar$  is the reduced Planck's constant,  $r_e$  is the classical electron radius,  $m_e$  is the electron mass,  $c$  is the speed of light,  $\alpha_k$  is the radiation damping constant for mode  $k = I, II, III$ ,  $E_{k5}$  is the 5<sup>th</sup> component of the normalized eigenvector for the mode  $k$  at the location of this period. A relative small contributions from sideways photons can be included as well,

$$\langle |A_{\pm k}|^2 \rangle_{sideways} = C_L \frac{\gamma^3 |E_{k(1,3)}(s)|^2}{c\alpha_k} \frac{2\hat{B}_y^3 \lambda_l}{3\pi(B\rho)^3}, \quad (\text{B5})$$

Here  $E_{k(1,3)}(s)$  is the 1<sup>st</sup> or 3<sup>rd</sup> component of the normalized  $k^{th}$  mode's eigenvector in the horizontal or vertical plane. Here all photon emission events are assumed to be uncorrelated. The intrinsic dispersion effect [42] is ignored because it is negligible comparing with bending magnets in the third and fourth generation light source rings.

When calculating closed orbit, nonvanishing elements for one period in the 7<sup>th</sup> column are

$$\begin{aligned} m_{67} &= -\frac{C_\gamma E^3 \hat{B}_y^2 \lambda_l}{2\pi(B\rho)^2} \\ m_{77} &= 1. \end{aligned} \quad (\text{B6})$$

Unlike bending magnets,  $m_{27}$  for a complete wiggler period is zero due to its alternating field polarities.

- 
- [1] C. Steier, A. Allézy, A. Anders, K. Baptiste, E. Buice, K. Chow, G. Cutler, R. Donahue, D. Filippetto, J. Harkins, *et al.*, "Status of the conceptual design of als-u," in *9th International Particle Accelerator Conference (2018)* pp. 4134–4137.
- [2] M. Borland, L. Emery, R. Lindberg, V. Sajaev, Y. Sun, and A. Xiao, "Overview of lattice design and evaluation for the aps upgrade," *ICFA Beam Dynamics Newsletter* **71** (2017).
- [3] P. Bryant, *A simple theory for betatron coupling*, Tech. Rep. (CERN, Geneva, 1975).
- [4] G. Guignard, "Linear coupling in storage rings with radiating particles," CERN ISR—BOM/79-30, LEP note 154 (1979).
- [5] A. Franchi, L. Farvacque, J. Chavanne, F. Ewald, B. Nash, K. Scheidt, and R. Tomás, "Vertical emittance reduction and preservation in electron storage rings via resonance driving terms correction," *Phys. Rev. ST Accel. Beams* **14**, 034002 (2011).
- [6] E. Courant and H. Snyder, "Theory of the alternating-gradient synchrotron," *Annals of physics* **3**, 1–48 (1958).
- [7] I. Borchardt, E. Karantzoulis, H. Mais, and G. Ripken, "Calculation of beam envelopes in storage rings and transport systems in the presence of transverse space charge effects and coupling," *Zeitschrift für Physik C Particles and Fields* **39**, 339–349 (1988).
- [8] F. Willeke and G. Ripken, "Methods of beam optics," in *AIP Conference Proceedings*, Vol. 184 (American Institute of Physics, 1989) pp. 758–819.
- [9] V. Lebedev and S. Bogacz, "Betatron motion with coupling of horizontal and vertical degrees of freedom," *Journal of Instrumentation* **5**, P10010 (2010).
- [10] D. Edwards and L. Teng, "Parametrization of linear coupled motion in periodic systems," *IEEE Transactions on nuclear science* **20**, 885–888 (1973).
- [11] Y. Luo, "Linear coupling parametrization in the

- action-angle frame,” *Physical Review Special Topics-Accelerators and Beams* **7**, 124001 (2004).
- [12] A. Wolski, “Alternative approach to general coupled linear optics,” *Phys. Rev. ST Accel. Beams* **9**, 024001 (2006).
- [13] G. Guignard, “The general theory of all sum and difference resonances in a three-dimensional magnetic field in a synchrotron,” (1976).
- [14] A. Chao, “Evaluation of beam distribution parameters in an electron storage ring,” *Journal of Applied Physics* **50**, 595–598 (1979).
- [15] A. Chao, “Evaluation of radiative spin polarization in an electron storage ring,” *Nuclear Instruments and Methods* **180**, 29–36 (1981).
- [16] A. Chao, “SLIM – a formalism for linear coupled systems,” *Chinese Physics C* **33**, 115 (2009).
- [17] K. Ohmi, K. Hirata, and K. Oide, “From the beam-envelope matrix to synchrotron-radiation integrals,” *Physical Review E* **49**, 751 (1994).
- [18] K. Hirata, “An introduction to sad,” (1988).
- [19] A. Terebilo, “Accelerator modeling with matlab accelerator toolbox,” in *PACS2001. Proceedings of the 2001 Particle Accelerator Conference (Cat. No. 01CH37268)*, Vol. 4 (IEEE, 2001) pp. 3203–3205.
- [20] A. Chao, “Lecture notes on special topics in accelerator physics: SLIM formalism–orbital motion,” <https://www.slac.stanford.edu/~achao/SLIM1.pdf>.
- [21] “MAD - Methodical Accelerator Design,” <https://madx.web.cern.ch/madx/>.
- [22] M. Sands, “Physics of electron storage rings: An introduction,” SLAC-121 (1970).
- [23] D. Sagan and D. Rubin, “Linear analysis of coupled lattices,” *Physical Review Special Topics-Accelerators and Beams* **2**, 074001 (1999).
- [24] M. Borland, “elegant: A Flexible SDDS-Compliant Code for Accelerator Simulation,” *Advanced Photon Source, LS-287* (2000).
- [25] H. Grote, C. Iselin, E. Keil, and J. Niederer, “The mad program,” in *Proceedings of the 1989 IEEE Particle Accelerator Conference (IEEE, 1989)* pp. 1292–1294.
- [26] H. Yoshida, “Construction of higher order symplectic integrators,” *Phys. Lett.* **A150**, 262–268 (1990).
- [27] D. Carey, K. Brown, and F. Rothacker, “Third-Order TRANSPORT with MAD Input-A Computer Program for Designing Charged Particle Beam Transport Systems,” *Fermilab-Pub-95/069, SLAC-R-95-462, UC-414* (1998).
- [28] A. Berz, “Differential algebraic description of beam dynamics to very high orders,” *Part. Accel.* **24**, 109–124 (1988).
- [29] T. Lavine, J. Seeman, W. Atwood, T. Himel, A. Petersen, and C. Adolphsen, *Beam determination of quadrupole misalignments and beam position monitor biases in the SLC linac*, Tech. Rep. (Stanford Linear Accelerator Center, 1988).
- [30] G. Portmann, D. Robin, and L. Schachinger, “Automated beam based alignment of the als quadrupoles,” in *Proceedings Particle Accelerator Conference*, Vol. 4 (IEEE, 1995) pp. 2693–2695.
- [31] A. Chao and X. Deng, personal communication (2021).
- [32] D. Ratner and A. Chao, “Steady-state microbunching in a storage ring for generating coherent radiation,” *Physical review letters* **105**, 154801 (2010).
- [33] C. Du, J. Wang, D. Ji, and S. Tian, “A conceptual design study of generating locally-round beam in a diffraction-limited storage ring using skew quadrupole triplets,” *Nuclear Instruments and Methods in Physics Research Section A: Accelerators, Spectrometers, Detectors and Associated Equipment* **992**, 165052 (2021).
- [34] J. Safranek, “Experimental determination of storage ring optics using orbit response measurements,” *Nuclear Instruments and Methods in Physics Research Section A: Accelerators, Spectrometers, Detectors and Associated Equipment* **388**, 27–36 (1997).
- [35] M. Borland, V. Sajaev, L. Emery, and A. Xiao, “Direct methods of optimization of storage ring dynamic and momentum aperture,” *Proceedings of PAC09, TH6PFP062* (2009).
- [36] L. Yang, Y. Li, W. Guo, and S. Krinsky, “Multiobjective optimization of dynamic aperture,” *Physical Review Special Topics-Accelerators and Beams* **14**, 054001 (2011).
- [37] X. Huang and J. Safranek, “Nonlinear dynamics optimization with particle swarm and genetic algorithms for spear3 emittance upgrade,” *Nuclear Instruments and Methods in Physics Research Section A: Accelerators, Spectrometers, Detectors and Associated Equipment* **757**, 48–53 (2014).
- [38] X. Huang and J. Safranek, “Online optimization of storage ring nonlinear beam dynamics,” *Physical Review Special Topics-Accelerators and Beams* **18**, 084001 (2015).
- [39] F. Iselin, “Lie transformations and transport equations for combined-function dipoles,” *Part. Accel.* **17**, 143–155 (1984).
- [40] K. Halbach, “Design of permanent multipole magnets with oriented rare earth cobalt material,” *Nuclear instruments and methods* **169**, 1–10 (1980).
- [41] L. Smith, “Effects of wigglers and undulators on beam dynamics,” LBL-21391, ESG-18 (1986).
- [42] Y. Zhang, X. Deng, Z. Pan, Z. Li, K. Zhou, W. Huang, R. Li, C. Tang, and A. Chao, “Ultralow longitudinal emittance storage rings,” *Physical Review Accelerators and Beams* **24**, 090701 (2021).